Fourth Asia-Pacific Conference on FRP in Structures (APFIS 2013)
11-13 December 2013, Melbourne, Australia

INFLUENCE OF SILICA FUME ON STRESS-STRAIN BEHAVIOR OF FRP-CONFINED HSC

J. C. Lim [1] and T. Ozbakkaloglu [2]
[1, 2] School of Civil, Environmental and Mining Engineering, University of Adelaide, Australia.

ABSTRACT

Confinement of high-strength concrete (HSC) columns with fiber reinforced polymer (FRP) composites has been receiving increasing research attention due to the advantageous engineering properties offered by the composite system. The use of silica fume as a concrete additive is a widely accepted practice in producing HSC. However, the influence of presence and amount of silica fume on the efficiency of FRP confinement has not been clearly understood. This paper presents results of an experimental study on the influence of silica fume on FRP-confined HSC. Nine aramid FRP (AFRP)-confined and nine unconfined concrete cylinders were tested under axial compression. The change in the mechanical properties of FRP-confined and unconfined HSC with silica fume amount was investigated. The results indicate that the compressive strength of unconfined concrete increases with an increase in the amount of silica fume. However, this increase comes at a cost of increased concrete brittleness, which adversely affects the effectiveness of FRP confinement. These observations were further validated with 93 test results of FRP-confined HSC assembled from the published literature. The additional results from the database allowed further observations to be made on the influence of silica fume on the compressive behavior of FRP-confined HSC. This paper presents the findings of these investigations.

KEYWORDS

Fiber reinforced polymer (FRP); confinement; compression; high-strength concrete (HSC); silica fume; stress-strain relations.

INTRODUCTION

The popularity of higher strength concretes in the construction industry has been on a steady incline during the last two decades due to the superior performance and economy offered by high-strength concrete (HSC) over normal-strength concrete (NSC) in a large number of structural engineering applications. The use of FRP for confinement of HSC leads to high-performance columns that exhibit very ductile behavior as was demonstrated in Ozbakkaloglu and Saatcioglu (2006; 2007) and Idris and Ozbakkaloglu (2013). Silica fume is one of the most popular pozzolans used to increase concrete strength. Although several studies have reported that silica fume alters the brittleness of confined concrete (Setunge et al. 1993; Samani and Attard 2012), its influence on the behavior of confined concrete has been difficult to quantify due to the limited results and controversial experimental observations found from existing triaxial compression tests of HSC (Xie et al. 1995; Attard and Setunge 1996; Ansari and Li 1998; Samani and Attard 2012). In FRP-confined HSC, the influence of silica fume is much less understood. Silica fume have been used in a number of existing experimental studies on FRP-confined concrete (e.g. Berthet et al. 2005; Mandal et al. 2005; Almusallam 2007; Ozbakkaloglu and Vincent 2013; Vincent and Ozbakkaloglu 2013a; Vincent and Ozbakkaloglu 2013b) to produce desirable concrete strengths. Xiao et al. (2010) pointed to the potential influence of silica fume on the compressive behavior of FRP-confined concrete based on the comparison of results available in the literature. However, none of the existing studies attempted to establish the influence of silica fume on the behavior of confined concrete. This paper presents the results of the first-ever experimental study that was undertaken to address this research gap, where the changes in the axial stress-strain behavior and ultimate conditions of FRP-confined HSC with silica fume were investigated through axial compression tests.

EXPERIMENTAL PROGRAM

Test Specimens and Materials

Nine FRP-confined and nine unconfined control concrete cylinders were manufactured and tested under monotonic axial compression. All of the specimens were 152 mm in diameter and 305 mm in height. The influence of silica fume on mechanical properties of the confined and unconfined specimens was investigated using three separate batches of

concrete mixes containing different percentage replacements of cement with silica fume. The percentages of silica fume that replaced cement were 0%, 8%, and 16% by weight. All of the concrete mixes had constant cementitious binder content at 550 kg/m^3. Ordinary Portland cement and silica fume were used as the cementitious binder materials. Details of the mix proportions of the three batches of concrete containing different levels of silica fume are given in Table 1. Crushed bluestone gravel of 10 mm maximum size and graded sand were used as the aggregates. A fixed water-cementitious binder ratio of 0.27 was used in all three batches. Carboxylic ether polymer based superplasticiser was used at a constant dosage of 5.5% by weight of the cementitious binder. The superplasticiser contained 80% water by weight. The details and test results of the unconfined specimens are given in Table 2.

Table 1. Mix proportions of concrete containing different levels of silica fume

Batch	1	2	3
Cement (kg/m^3)	550	506	462
Silica fume (kg/m^3)	0	44	88
Sand (kg/m^3)	700	700	700
Gravel (kg/m^3)	1050	1050	1050
Water (kg/m^3)	124	124	124
Superplasticiser (kg/m^3)	30	30	30
Water-binder ratio	0.270	0.270	0.270
Superplasticiser-binder ratio	0.055	0.055	0.055
Silica fume-binder ratio	0.000	0.080	0.160
Slump height (m)	0.240	0.215	0.220

The FRP-confined specimens were prepared using a manual wet lay-up process by wrapping epoxy resin impregnated aramid fiber sheets around the concrete cylinders in the hoop direction. The specimens were confined with 6 layers of AFRP, which were applied through two aramid fiber sheets that terminated at the same overlap region of 150 mm length. Three nominally identical specimens were tested for each unique specimen configuration, and the FRP-confined specimens were tested on the same day with the companion unconfined specimens. The axial compression tests were performed using a 5000-kN capacity universal testing machine. During the initial elastic stage of the behavior, the loading was applied with load control at 5 kN per second, whereas displacement control was used at 0.004 mm per second beyond the initial softening until specimen failure. Prior to testing, all specimens were capped at both ends to ensure uniform distribution of the applied pressure, and load was applied directly to the concrete core through the use of precision-cut high-strength steel plates. The hoop strains were measured using three unidirectional strain gauges placed at the mid-height at 120° spacing around the specimens outside the overlap region. The axial strains were measured using three different methods: (i) four linear variable displacement transformers (LVDTs) mounted at each corner of the steel loading platens with a gauge length of 305 mm; (ii) four LVDTs placed at the mid-height at a gauge length of 170 mm at 90° spacing along the circumference of specimens; (iii) three axial strain gauges with a gauge length of 20 mm placed at the mid-height at 120° spacing along the circumference. The strain gauge measurements were used to validate LVDT measurements at the early stages of loading. The mid-height LVDTs were used to compare the discrepancy in measurements recorded by the steel platen mounted LVDTs. The axial strains of specimens reported in this paper were established based on the deformations recorded by the steel-platen mounted LVDTs.

Table 2. Results of compression tests on unconfined specimens

Specimen	Concrete batch	Silica fume percentage (%)	f'_{co} (MPa)	Average f'_{co} (MPa)	ε_{co} (%)	Average ε_{co} (%)
B1-SF0-L0-1			89.9		0.24	
B1-SF0-L0-2	1	0	82.7	85.7	0.25	0.24
B1-SF0-L0-3			84.6		0.24	
B2-SF8-L0-1			114.1		0.26	
B2-SF8-L0-2	2	8	113.8	112.4	0.28	0.27
B2-SF8-L0-3			109.4		0.26	
B3-SF16-L0-1			115.1		0.26	
B3-SF16-L0-2	3	16	114.3	113.5	0.27	0.26
B3-SF16-L0-3			111.0		0.25	

The test results of the AFRP-confined specimens are given in Table 3, which include: the compressive strength and ultimate axial strain of the specimens (f'_{cc} and ε_{cu}); hoop rupture strain ($\varepsilon_{h,rup}$); strength and strain enhancement ratios (f'_{cc}/f'_{co} and $\varepsilon_{cu}/\varepsilon_{co}$); and hoop strain reduction factor ($k_{\varepsilon,f}$). The hoop strain reduction factor ($k_{\varepsilon,f}$) was calculated as the ratio of the hoop rupture strain ($\varepsilon_{h,rup}$) to ultimate tensile strain of fiber (ε_f). The specimens in

Tables 2 and 3 were labeled as follows: letters B, SF and L were used to represent the test parameters, namely the concrete batch, silica fume percentage, and number of FRP layers, respectively. Each letter was followed by a number that was used to represent the value of that particular parameter for a given specimen. The last number in the specimen designation (i.e., 1, 2 or 3) was used to make distinction between three nominally identical specimens.

Table 3. Results of compression tests on confined specimens

Specimen	f'_{cc} (MPa)	ε_{cu} (%)	$\varepsilon_{h,rup}$ (%)	f'_{cc}/f'_{co}	Average f'_{cc}/f'_{co}	$\varepsilon_{cu}/\varepsilon_{co}$	Average $\varepsilon_{cu}/\varepsilon_{co}$	$k_{\varepsilon,f}$	Average $k_{\varepsilon,f}$
B1-SF0-L6-1	166.2	2.02	1.50	1.94		8.25		0.68	
B1-SF0-L6-2	168.0	2.18	1.48	1.96	1.94	8.89	8.56	0.67	0.67
B1-SF0-L6-3	165.2	2.09	1.45	1.93		8.54		0.66	
B2-SF8-L6-1	165.5	1.97	1.37	1.47		7.38		0.62	
B2-SF8-L6-2	168.4	1.74	1.48	1.50	1.47	6.51	6.97	0.68	0.66
B2-SF8-L6-3	163.1	1.87	1.47	1.45		7.01		0.67	
B3-SF16-L6-1	186.5	2.04	1.50	1.64		7.89		0.68	
B3-SF16-L6-2	170.7	1.75	1.19	1.50	1.57	6.77	7.38	0.54	0.63
B3-SF16-L6-3	178.5	1.94	1.45	1.57		7.47		0.66	

The properties of the unidirectional aramid fiber sheets used for wrapping the specimens are provided in Table 4. The table reports both the manufacturers supplied fiber properties and the tensile tested FRP composite properties. The tensile properties of the FRP made from these aramid fiber sheets and epoxy resin were determined from flat coupon tests in accordance with ASTM D3039 (2008). A total of three flat coupon specimens were made using wet layout technique in a high-precision mould with 1 mm thickness and 25 mm width. The coupons had 138 mm clear span with each end bonded with two 0.5 mm by 85 mm aluminum tabs for stress transfer during tensile tests. Each coupon was instrumented with two 20 mm strain gauges at mid height, with one on each side, for the measurement of the longitudinal strains. The coupons were allowed to cure in laboratory environment for at least 7 days prior to testing. The tensile test specimens were tested using a screw-driven tensile test machine that has a peak capacity of 200 kN. The load was applied at a constant cross-head movement rate of 0.03 mm per second. The test results from the flat coupon specimens, calculated based on nominal fiber thicknesses and actual coupon widths, are reported in Table 4. As evident from Table 4, the average rupture strain obtained from the tensile coupon tests was slightly lower than that reported by the manufacturer.

Table 4. Material properties of fibers and FRP composites

Type	Nominal thickness t_f (mm/ply)	Provided by manufacturers			Obtained from flat FRP coupon tests		
		Tensile strength f_f (MPa)	Ultimate tensile strain ε_f (%)	Elastic modulus E_f (GPa)	Tensile strength f_{frp} (MPa)	Ultimate tensile strain ε_{frp} (%)	Elastic modulus E_{frp} (GPa)
Aramid	0.200	2600	2.20	118.2	2390	1.86	128.5

TEST RESULTS AND DISCUSSION

Ultimate conditions

The ultimate condition of FRP-confined concrete is often characterized as the ultimate axial stress and strain of concrete recorded at the rupture of the FRP jacket. This makes the relationship between the ultimate axial stress (f'_{cu}), ultimate axial strain (ε_{cu}) and hoop rupture strain ($\varepsilon_{h,rup}$) an important one. Table 2 shows that the unconfined concrete strengths (f'_{co}) of specimens increased from 85.7 MPa to 112.4 MPa with an increase in silica fume content from 0% to 8%. Only a slight improvement in strength was observed with a further increase in silica fume content from 8% to 16%. As illustrated in Table 3, the increase in the concrete strength (f'_{co}) from 85.7 MPa to 112.4 MPa resulted in reduction in the strength enhancement ratio (f'_{cc}/f'_{co}) of AFRP-confined concrete from 1.94 to 1.47. The table also shows that the strength enhancement ratio (f'_{cc}/f'_{co}) varied slightly (i.e. from 1.47 to 1.57) with the change in silica fume content from 8% to 16%. Table 3 further illustrates that the strain enhancement ratio of ($\varepsilon_{cu}/\varepsilon_{co}$) of AFRP-confined concrete reduced from 8.56 to 6.97 with a change in the silica fume content from 0% to 8%. No further reduction in $\varepsilon_{cu}/\varepsilon_{co}$ was observed with a further increase in silica fume content to 16%. These observations indicate that for a given water-binder ratio, presence of silica fume increases the unconfined concrete strength (f'_{co}) and corresponding axial strain (ε_{co}), and this increase is not directly proportional to the amount of silica fume. The observations also indicate that the improvement in unconfined concrete strength comes at the cost of reduced strength and strain enhancement ratios (f'_{cc}/f'_{co} and $\varepsilon_{cu}/\varepsilon_{co}$).

The recorded hoop rupture strains ($\varepsilon_{h,rup}$) and calculated strain reduction factors ($k_{\varepsilon,f} = \varepsilon_{h,rup}/\varepsilon_f$) from the test results are provided in Table 3. It has been discussed previously in a number of studies (e.g. De Lorenzis and Tepfers 2003; Harries and Carey 2003; Lam and Teng 2004; Ozbakkaloglu and Oehlers 2008; Vincent and Ozbakkaloglu 2013a) that the ultimate hoop strain ($\varepsilon_{h,rup}$) reached in the FRP jacket is often smaller than the ultimate tensile strain of the fibers (ε_f), which necessitates the use of a strain reduction factor ($k_{\varepsilon,f}$) in the determination of the actual confining pressures. A closer inspection of the results reported in Table 3 leads to the observation that the $k_{\varepsilon,f}$ values slightly reduces with the increase in unconfined concrete strength (f'_{co}), which is in agreement with the previous finding reported in Lim and Ozbakkaloglu (2013).

Axial stress-strain behavior

The different stages observed on a typical axial stress-train curve of the specimens are illustrated in Fig. 1. Axial stress-strain curves of all the test specimens are shown in Figs. 2(a) to 2(c). The curves of the companion specimens shown in Figs. 2(a) and 2(c) were represented through the use of three different line styles. As evident from Figs. 2(a) to 2(c), FRP-confined HSC can exhibit highly ductile compressive behavior. It is well established that the FRP-confined concrete exhibits a monotonically ascending curve, which consists of a parabolic first portion and a nearly straight-line second portion (e.g., Specimen B1-SF0-L6 in Fig. 2(a)), if the level of confinement exceeds a certain threshold (Ozbakkaloglu 2013a; 2013b). On the other hand, when the confinement level is below this threshold, the first ascending branch is followed by a second branch that exhibits an initial softening region (e.g., Specimens B2-SF8-L6 and B3-SF16-L6 in Figs. 2(b) and 2(c)). The confinement requirements and threshold conditions for distinguishing the types of curves were discussed in detail in Lim and Ozbakkaloglu (2013).

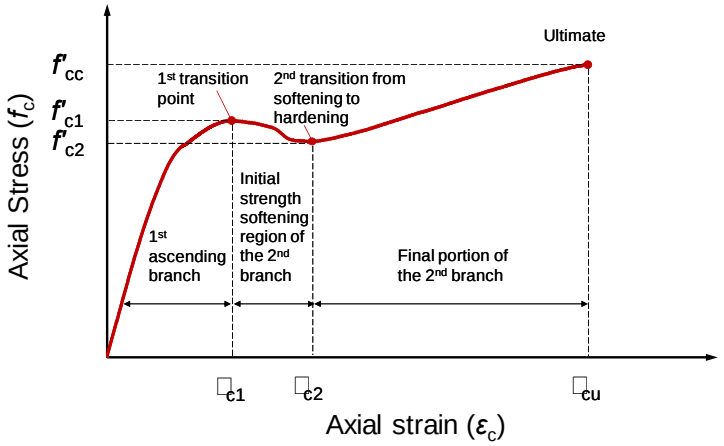

Figure 1. Illustration of different stages of axial stress-strain curves

It can be observed from Figs. 2(b) and 2(c), the specimens with 8% and 16% silica fume contents experienced a sudden drop in strength starting at the first transition point on their stress-strain curves. In contrast, no strength loss was observed in specimens with 0% silica fume content, as illustrated in Fig. 2(a). This initial softening phenomenon can be attributed to the increased concrete brittleness with increasing concrete strength, which alters the concrete crack patterns from heterogenic microcracks to localized macrocracks (Ozbakkaloglu and Akin 2012; Lim and Ozbakkaloglu 2013). This change in cracking pattern results in a more rapid and uncontrolled expansion which gradually activates the confinement mechanism (Ozbakkaloglu and Vincent 2013). As a result, the confinement mechanism in HSC gets activated only after significant amount of damage is sustained by the concrete. As evident from Figs. 2(b) and 2(c), the magnitude of the strength loss observed along the initial strength softening region was more significant for the specimens with higher silica fume content. These observations indicate that the use of silica fume increases the strength of unconfined concrete at the cost of increased concrete brittleness, which in turn increases the magnitude of initial strength loss observed in the stress-strain curves of these specimens.

EXPERIMENTAL TEST DATABASE

In addition to observations made from the experimental test results reported in this paper, the authors have undertaken extensive an extensive review of existing studies of FRP-confined HSC available in the literature. The test results were collected to form a large experimental database that catalogued 237 test datasets (Lim and Ozbakkaloglu 2013). Including the reported test results, 93 datasets that contain details of the silica fume content used in the concrete mixtures were studied to establish the influence of silica fume on strength and strain enhancement effects of FRP-confined HSC. The strength and strain enhancement coefficients (k_1 and k_2) of the

specimens were calculated using the model proposed in Lim and Ozbakkaloglu (2013). As illustrated by the trendlines of Figs. 3(a) and 3(b), the strength and strain enhancement coefficients (k_1 and k_2) decline with the increase in silica fume amount in the concrete mix. This supports the findings of the experimental study that the use of silica fume increases the strength of the concrete, at the cost of increased concrete brittleness, which in turn reduces the effectiveness of FRP confinement.

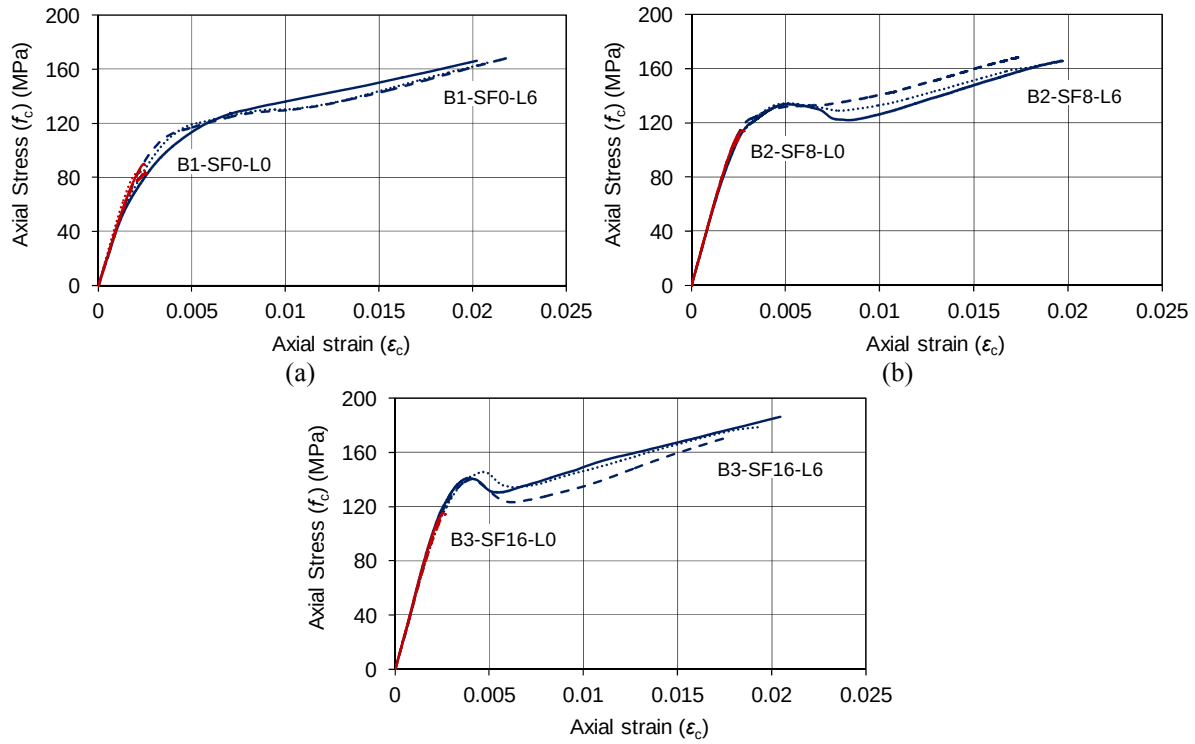

Figure 2. Influence of silica fume on axial stress-strain curves: a) 0% silica fume; b) 8% silica fume; c) 16% silica fume

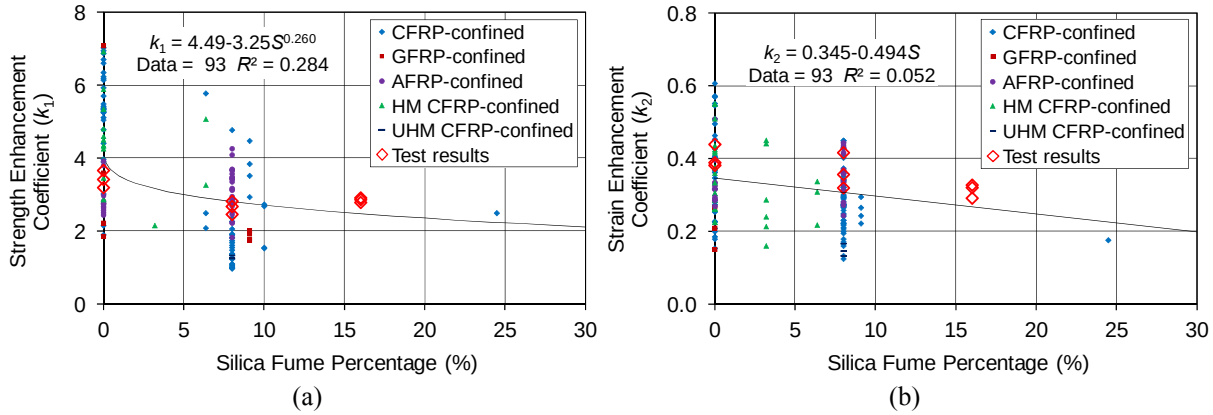

Figure 3. Variations of: (a) strength enhancement coefficient (k_1), and (b) strain enhancement coefficient (k_2) with silica fume percentage

CONCLUSIONS

This paper has presented the results of an experimental study on the influence of silica fume on the axial compressive behavior of FRP-confined HSC. Additional test results of FRP-confined HSC were collected from existing studies to form a large database. The combined results were used to study the influence of silica fume on the stress-strain behavior and ultimate conditions of FRP-confined HSC. Based on the results and discussions presented in the paper, the following conclusions can be drawn:

1. Sufficiently confined HSC with and without silica fume can exhibit highly ductile compressive behavior.
2. Silica fume improves the strength of concrete, at the cost of increased concrete brittleness, which in turn reduces the effectiveness of FRP confinement.

3. FRP-confined concrete can exhibit a monotonically ascending stress-strain curve or a curve with an initial strength loss at the transition region. Due to the increased concrete strength and brittleness that result from the addition of silica fume to the concrete mix, these strength losses are more significant for concretes containing silica fume.
4. The hoop strain reduction factor ($k_{\varepsilon,f}$) is observed to slightly decrease with an increase in concrete strength (f'_{co}) resulting from the addition of silica fume to the mix. Additional tests are required to better understand this influence.

REFERENCES

Almusallam, T. H. (2007). "Behavior of normal and high-strength concrete cylinders confined with E-glass/epoxy composite laminates." *Composites Part B-Engineering*, 38(5-6), 629-639.

Ansari, F. and Li, Q. B. (1998). "High-strength concrete subjected to triaxial compression." *ACI Materials Journal*, 95(6), 747-755.

ASTM-D3039 (2008). "Standard test method for tensile properties of polymer matrix composite materials." *D3039/D3039M-08*, West Conshohocken, PA.

Attard, M. M. and Setunge, S. (1996). "Stress-strain relationship of confined and unconfined concrete." *ACI Materials Journal*, 93(5), 432-442.

Berthet, J. F., Ferrier, E. and Hamelin, P. (2005). "Compressive behavior of concrete externally confined by composite jackets. Part A: experimental study." *Construction and Building Materials*, 19(3), 223-232.

De Lorenzis, L. and Tepfers, R. (2003). "Comparative study of models on confinement of concrete cylinders with fiber-reinforced polymer composites." *Journal of Composites for Construction, ASCE,* 7(3), 219-237.

Harries, K. A. and Carey, S. A. (2003). "Shape and "gap" effects on the behavior of variably confined concrete." *Cement and Concrete Research*, 33(6), 881-890.

Idris, Y. and Ozbakkaloglu, T. (2013). "Seismic behavior of high-strength concrete-filled FRP tube columns." *Journal of Composites for Construction, ASCE,* doi: 10.1061/(ASCE)CC.1943-5614.0000388.

Lam, L. and Teng, J. G. (2004). "Ultimate condition of fiber reinforced polymer-confined concrete." *Journal of Composites for Construction, ASCE,* 8(6), 539-548.

Lim, J. C. and Ozbakkaloglu, T. (2013). "Confinement model for FRP-confined high-strength concrete." *Journal of Composites for Construction, ASCE,* doi: 10.1061/(ASCE)CC.1943-5614.0000376.

Mandal, S., Hoskin, A. and Fam, A. (2005). "Influence of concrete strength on confinement effectiveness of fiber-reinforced polymer circular jackets." *ACI Structural Journal*, 102(3), 383-392.

Ozbakkaloglu, T. (2013a). "Axial compressive behavior of square and rectangular high-strength concrete-filled FRP tubes." *Journal of Composites for Construction, ASCE,* 17(1), 151-161.

Ozbakkaloglu, T. (2013b). "Behavior of square and rectangular ultra high-strength concrete-filled FRP tubes under axial compression." *Composites Part B: Engineering.*, 54, 97-111.

Ozbakkaloglu, T. and Akin, E. (2012). "Behavior of FRP-confined normal- and high-strength concrete under cyclic axial compression." *Journal of Composites for Construction, ASCE,* 16(4), 451-463.

Ozbakkaloglu, T. and Oehlers, D. J. (2008). "Concrete-filled square and rectangular FRP tubes under axial compression." *Journal of Composites for Construction, ASCE,* 12(4), 469-477.

Ozbakkaloglu, T. and Saatcioglu, M. (2006). "Seismic behavior of high-strength concrete columns confined by fiber-reinforced polymer tubes." *Journal of Composites for Construction, ASCE,* 10(6), 538-549.

Ozbakkaloglu, T. and Saatcioglu, M. (2007). "Seismic performance of square high-strength concrete columns in FRP stay-in-place formwork." *Journal of Structural Engineering, ASCE,* 133(1), 44-56.

Ozbakkaloglu, T. and Vincent, T. (2013). "Axial compressive behavior of circular high-strength concrete-filled FRP tubes." *Journal of Composites for Construction, ASCE,* doi: 10.1061/(ASCE)CC.1943-5614.0000410.

Samani, A. K. and Attard, M. M. (2012). "A stress-strain model for uniaxial and confined concrete under compression." *Engineering Structures*, 41, 335-349.

Setunge, S., Attard, M. M. and Darvall, P. L. (1993). "Ultimate strength of confined very high-strength concretes." *ACI Structural Journal*, 90(6), 632-641.

Vincent, T. and Ozbakkaloglu, T. (2013a). "Influence of concrete strength and confinement method on axial compressive behavior of FRP confined high- and ultra high-strength concrete." *Composites Part B*, 50, 413–428.

Vincent, T. and Ozbakkaloglu, T. (2013b). "Influence of fiber orientation and specimen end condition on axial compressive behavior of FRP-confined concrete." *Construction and Building Materials*, 47, 814-826.

Xiao, Q. G., Teng, J. G. and Yu, T. (2010). "Behavior and Modeling of Confined High-Strength Concrete." *Journal of Composites for Construction, ASCE,* 14(3), 249-259.

Xie, J., Elwi, A. E. and Macgregor, J. G. (1995). "Mechanical-properties of high-strength concretes containing silica fume." *ACI Materials Journal*, 92(2), 135-145.